THE JOURNAL OF BIOLOGICAL CHEMISTRY VOL. 282, NO. 12, pp. 8926–8934, March 23, 2007

The Characterization and Role of Zinc Binding in Yeast Cox4*[S]

Received for publication, November 3, 2006, and in revised form, December 19, 2006 Published, JBC Papers in Press, January 10, 2007, DOI 10.1074/jbc.M610303200

H. Jerome Coyne III[‡], Simone Ciofi-Baffoni[§], Lucia Banci[§], Ivano Bertini[§], Limei Zhang[¶], Graham N. George[¶], and Dennis R. Winge[‡1]

From the [‡]University of Utah Health Sciences Center, Departments of Medicine and Biochemistry, Salt Lake City, Utah 84132, [§]Centro Risonanze Magnetiche, University of Florence, Via Luigi Sacconi 6, 50019 Sesto Fiorentino (Florence), Italy, and [¶]University of Saskatchewan, Saskatoon S7N 5E2, Canada

Yeast Cox4 is a zinc binding subunit of cytochrome *c* oxidase. Cox4 is the only cofactor-containing subunit that is not directly part of the catalytic core of the enzyme located in the mitochondrial inner membrane. The Zn(II) site is shown to be distinct from the bovine ortholog, as it results from the x-ray structure of the entire cytochrome *c* oxidase in having a single histidyl residue and three conserved cysteines residues in the coordination sphere. Substitutions at the Cys ligand positions result in nonfunctional Cox4 proteins that fail to lead to cytochrome oxidase assembly. Limited function exists in His-119 mutants when overexpressed. Zn(II) binding in Cox4 is, therefore, important for the stability of the complex. The solution structure of yeast Cox4 elucidated by multidimensional NMR reveals a C-terminal globular domain consisting of two β sheets analogous to the bovine ortholog except the loop containing the coordinating His in the yeast protein and the fourth Cys in the bovine protein are in different positions in the two structures. The conformation of this loop is dictated by the different sequence position of the fourth coordinating zinc ligand. The Zn(II) ion is buried within the domain, consistent with its role in structural stability. Potential functions of this matrix-facing subunit are discussed.

Cytochrome *c* oxidase (CcO),[2] or complex IV, is the terminal enzyme in the respiratory chain. Complex IV is located in the mitochondria of eukaryotes, where it is embedded within the inner membrane (IM). CcO catalyzes the reduction of molecular oxygen to water (1). The catalytic cycle of CcO pumps eight protons from the matrix to both the reaction center and into the inner membrane space. Four of the protons are directed to the heme a_3-Cu_B reaction center to participate in the formation of water. The remaining protons are released into the inner membrane space to create a proton gradient, which is used to drive the synthesis of ATP via ATP synthase. The bulk of ATP in eukaryotic cells is produced through the respiratory chain. The importance of the pathway has generated interest in understanding the mechanism of CcO assembly and the function of individual subunits in forming the oligomeric holoenzyme.

The subunits of CcO are encoded by both nuclear and mitochondrial genes. The core subunits, Cox1–3, are mitochondrial gene products and either bind cofactors involved in the electron transport pathway or are involved in proton translocation (2, 3). Cox1 contains the heme *a*, heme a_3, and the mononuclear Cu_B site. One histidine ligand bridges Cu_B and heme a_3, having a role in water formation (4). Cox2 contains the binuclear Cu_A site responsible for accepting the reducing electrons from cytochrome *c*. Cox3 is a core subunit containing no cofactors and has been proposed to regulate proton uptake through the D-channel (5).

The core CcO complex is surrounded by 10 small peripheral subunits, many of which consist of a single transmembrane helix. The peripheral subunits are encoded by the nuclear genome (6), but only a subset of these subunits shows sequence similarity between animals and yeast orthologs. Many of these subunits are functionally important, since deletion of genes in yeast for some peripheral subunits results in respiratory deficiency (6).

One conserved peripheral subunit is CoxVb, designated Cox4 in *Saccharomyces cerevisiae*. Cox4 is an essential subunit of CcO as the enzyme fails to assemble in *cox4*Δ cells, and core subunits Cox1 and Cox2 fail to accumulate, thus inducing respiratory deficiency (7, 12). The importance of CoxVb is apparent from the crystal structure of bovine CcO, as the subunit is closely packed onto Cox1 and Cox3 on the matrix side of the IM (2). CoxVb does not penetrate the lipid bilayer. CoxVb coordinates a single Zn(II) ion through four cysteinyl residues (2). Because the nomenclature for this subunit varies between mammals and yeast, we will use the yeast Cox4 designation for this study as the focus of the work is on the yeast protein.

The physiological roles of Cox4 and Zn(II) coordination in CcO remain unclear. Zn(II) has been suggested to be a structural component of the subunit, but this has not been tested.

* This work was supported by NIEHS, National Institutes of Health Grant ES 03817 (to D. R. W.) We also acknowledge the support of PRIN-COFIN 2005 Prot. 2005039878 (to Genomica strutturale di metalloproteine e delle loro interazioni funzionali). Research at the University of Saskatchewan was supported in part by Canada Research Chair award (to G. N. G.), the University of Saskatchewan, the Province of Saskatchewan, the National Institutes of Health (Grant GM57375), the Natural Sciences and Engineering Research Council (Canada) (Grant 283315), and the Canadian Institute of Health Research. The costs of publication of this article were defrayed in part by the payment of page charges. This article must therefore be hereby marked "*advertisement*" in accordance with 18 U.S.C. Section 1734 solely to indicate this fact.

[S] The on-line version of this article (available at http://www.jbc.org) contains supplemental Tables S1–S3 and Figs. S1 and S2.

The atomic coordinates and structure factors (code 2ODX) have been deposited in the Protein Data Bank, Research Collaboratory for Structural Bioinformatics, Rutgers University, New Brunswick, NJ (http://www.rcsb.org/).

[1] To whom correspondence should be addressed. Tel.: 801-585-5103; Fax: 801-585-5469; E-mail: dennis.winge@hsc.utah.edu.

[2] The abbreviations used are: CcO, cytochrome *c* oxidase; IM, inner membrane; WT, wild type; EXAFS, x-ray absorption fine structure; NOE, nuclear Overhauser effect; HSQC, heteronuclear single quantum correlation; ROS, reactive oxygen species.

Yeast Cox4 has only three of the four conserved cysteinyl residues in its primary sequence (8).

The spectroscopic inertness of Zn(II) makes direct determination of its coordination environment difficult, but metal substitution is a useful alternative. Zn(II) prefers tetrahedral coordination geometry. Cd(II) and Co(II) can be substituted in zinc proteins, since they can be accommodated by the same coordination geometry and utilize similar donor ligands as Zn(II). ^{113}Cd(II) has a nuclear spin of ½ and is amenable to NMR analysis. The chemical shift observed of a cadmium nucleus is indicative of the coordination environment. A single one-dimensional measurement can provide clues as to which atoms are directly coordinated to the cadmium nucleus (9). Co(II) is a useful probe using electronic spectroscopy. Ligand to metal charge transfer bands and absorption in the visible region due to *d-d* transitions provide information on the coordination environment for both geometry and ligand atoms (10, 11).

We show in this report that yeast Cox4 binds Zn(II) through three cysteinyl residues and a single histidine. The structure of the C-terminal globular domain Cox4 reveals an overall fold similar to that of bovine CoxVb but with local structural difference on the loop accommodating the His ligand. A structural comparison of the conserved hydrophobic residues between the yeast and bovine homologues identify which of them can play a key role in the Cox4-Cox1 interaction.

MATERIALS AND METHODS

Strains and Vectors—The Δ*cox4* yeast strain was generously provided by Dr. A. Tzagoloff (12). The wild-type *COX4* was amplified from yeast genomic DNA by PCR such that 1000 base pairs upstream of the ATG translation start were included. The primers for the 5′ and 3′ ends of *COX4* were 5′-AAAAAGCTTCAGTGTGTATACCCTCC and 5′-AAAGGATCCTATAGATAGAGCAAAGCGTTCG, respectively. The PCR product was then restriction enzyme-digested with HindIII and BamHI for insertion into pRS425 (YEp plasmid with *LEU2* selection) and pRS415 (YCp plasmid with *LEU2* selection). Mutant *COX4* plasmids were constructed by PCR using the WT plasmid as a template. Primers were designed according to the protocol suggested by Stratagene, and the codons selected were based on the optimal frequency in *S. cerevisiae*.

COX4 used for recombinant studies in *Escherichia coli* was a construct encoding a truncated protein lacking the first 78 residues from the N terminus that form the mitochondrial targeting sequence and an extended segment in the bovine CoxVb structure. The truncated gene was inserted into pET20b+. Mutant variants were generated using the Stratagene QuikChange protocol. The codons selected for mutagenesis were based on the optimal frequency in *E. coli*. The recombinant had a three residue (MMA) N-terminal extension arising from the PCR protocol. The C-terminal truncate used in the ^{113}Cd NMR and cobalt and zinc titration studies terminated at Asn-75.

Yeast Analyses—Transformation of Δ*cox4* cells was by the lithium acetate procedure. The transformed yeast was grown to stationary phase in the synthetic glucose media to provide strain (+Ura) and plasmid (+Leu) selection. The cells were harvested, spun at 3000 rpm, and subsequently washed with sterile distilled water. Crude mitochondria of all transformed yeast samples were prepared according to the established protocol (13).

Immunoblotting was carried out on 12.5% SDS-PAGE gels with 20 μg of total mitochondrial protein applied per lane. Protein was quantified by the Bradford procedure (14). The separated protein was then electrolytically transferred to nitrocellulose. The primary antibody was mouse monoclonal yeast Cox4 (Molecular Probes), and the secondary antibody was anti-mouse horseradish peroxidase (Molecular Probes). The blot was developed using ECL reagents (Pierce). Porin and phosphoglycerolkinase (Pgk1) were used as markers for the mitochondrion and the cytoplasm using monoclonal antibodies (Molecular Probes).

Cox4 Purification—*COX4* expression plasmids were transformed into BL21(DE3) bacterial cells (Novagen) for recombinant protein production. Cultures were grown to an absorbance of ~0.6 at 37 °C before induction using 0.4 mM isopropyl 1-thio-β-D-galactopyranoside for 5 h at 30 °C. The cells were harvested and washed in 0.25 mM sucrose before storage at −80 °C. The cells were lysed by sonication in 2× phosphate-buffered saline containing 10 mM dithiothreitol. The sonication was done for five 1-min intervals at continuous full power with 1 min on ice in between the intervals. The lysate was clarified by centrifugation and filtered through a 0.22 μ membrane. The filtered lysate solution was concentrated (VIVA Spin cutoff 3000 Da) and successively diluted with sterile distilled water to bring the conductance down below 4 millisiemens.

Purification of Cox4 was performed with an AKTA fast protein liquid chromatography (Amersham Biosciences) using a Hi Prep DEAE FF anion exchange column. The wash buffer was 20 mM phosphate, pH 8.2, and elution was with a linear gradient up to 500 mM NaCl. The elution position of Cox4 was assessed by SDS-PAGE. Cox4 fractions were concentrated and injected onto a Hi Load Superdex 75 Prep Grade 26/60 size exclusion column equilibrated in 50 mM phosphate, 200 mM NaCl at pH 6.9. Cox4 eluted as a single band with minimal impurities as verified by SDS-PAGE analysis. Fractions containing pure Cox4 were pooled and concentrated (VIVA Spin 3000 Da) for analyses. The final stock solution of Cox4 was assessed for protein concentration at 280 nm using an extinction coefficient of 16,860 M^{-1} cm^{-1}. The zinc content was quantified by atomic absorption using a PerkinElmer Life Sciences AAnalyst 100.

Isotopically labeled proteins were produced and purified using the same procedures except the recombinant protein was expressed in M9 minimal medium. The broth contained $^{15}NH_4Cl$ (Isotec Inc.) as the nitrogen source and D-[^{13}C]glucose (Cambridge Isotope Laboratories, Inc.) as the carbon source. The cultures were induced with freshly prepared isopropyl 1-thio-β-D-galactopyranoside at a final concentration of 0.4 mM. The cultures also contained 0.1 mM exogenous $ZnSO_4$. The induction was carried out for 16–18 h at 30 °C.

X-ray Absorption Spectroscopy Data Collection and Analysis—X-ray absorption spectroscopy measurements were conducted at the Stanford Synchrotron Radiation Laboratory on beamline 9-3 using a Harmonic rejection mirror cutoff of 13 keV. The incident and transmitted x-ray intensities were monitored using N_2-filled ionization chambers, and x-ray absorption was

measured as the zinc Kα fluorescence excitation spectrum using an array of 30 germanium detectors (15). Samples were maintained at a temperature of 10 K using an Oxford instruments liquid helium flow cryostat, and four 45-min scans were accumulated. The x-ray energy was calibrated by simultaneous measurement of a zinc metal foil assuming a lowest energy inflection point of the metal to be 9659 eV. The energy threshold of the extended x-ray absorption fine structure (EXAFS) oscillations (k) was assumed to be 9675 eV. EXAFS were quantitatively analyzed by curve-fitting using the EXAFSPAK suite of computer programs. *Ab initio* theoretical phase and amplitude functions were calculated using the program FEFF Version 8.2 (16). No smoothing, filtering, or related operations were performed on the data.

Cobalt and Cadmium Spectroscopy—ApoCox4 was prepared by acid denaturation of purified Cox4 to a final pH of 2.0. The solution was gel-filtered on G-25 Sephadex in 0.01 N HCl to separate the protein from Zn(II). Apoprotein in acid was concentrated and titrated with $CoCl_2$ to 1.5 mol eq. The pH of the sample was adjusted to 7.2 using Tris base. The CoCox4 sample was scanned in a Beckman DU 640 spectrometer. The H119D Cox4 mutant was prepared anaerobically as the Co(II) complex was less stable aerobically.

ApoCox4 was also titrated with $^{113}CdCl_2$ and concentrated to 2 mM. The protein was loaded in a 3-mm NMR tube for analysis on a 500-MHz Varian ANOVA spectrometer with a MDBG-500 Nalorac 3-mm dual broad band gradient probe. The samples were referenced against $Cd(ClO_4)_2$. The frequency used was 110.924 MHz. Transients were collected overnight with a pulse width of 4 μs and a delay time of 1 s. Final spectrum processing included a line broadening factor of 150.

Multidimensional NMR and Structure Calculation—NMR spectra were acquired on Avance 800, 700, and 500 Bruker spectrometers operating at proton nominal frequencies of 800.13, 700.13, and 500.13 MHz, respectively. All the triple resonance (TXI 5-mm) probes used were equipped with pulsed field gradients along the z axis. The 800 and 500 MHz spectrometers were equipped with a triple resonance cryoprobe. The NMR experiments were recorded on ^{13}C,^{15}N- and ^{15}N-labeled Zn-Cox4 samples at 1–1.5 mM and at 298 K. The NMR experiments used for the backbone and the side-chain assignment and for obtaining structural restraints are summarized in supplemental Table S1. The ^{1}H, ^{13}C, and ^{15}N resonance assignments of Zn-Cox4 are reported in supplemental Table S2. The completeness of proton and heavy atoms assignments are 92 and 89%, respectively. All the three- and two-dimensional experiments were processed using the standard Bruker software (XWINNMR) and analyzed on PC Linux computers through the CARA program (17).

Structure calculations were performed with the software package ATNOS/CANDID/CYANA using as input the amino acid sequence, the chemical shift lists, and three ^{1}H,^{1}H NOE experiments; two-dimensional NOE spectroscopy (NOESY), three-dimensional ^{13}C-resolved NOESY, and three-dimensional ^{15}N-resolved NOESY were all recorded at 800 MHz with a mixing time of 100 ms. The standard protocol with seven cycles of peak picking using ATNOS (18), NOE assignment with CANDID (19), and structure calculation with CYANA-2.1 (20) was applied. ϕ and ψ dihedral angle constraints were derived from the chemical shift index (21). In each ATNOS/CANDID cycle, the angle constraints were combined with the updated NOE upper distance constraints in the input for the subsequent CYANA-2.1 structure calculation cycle. In the seventh ATNOS/CANDID/CYANA cycle, a total of 3226 NOE cross-peaks were assigned from 3751 peaks picked in the spectra of Zn-Cox4, which yielded 1172 meaningful NOE upper distance limits. The zinc ion was finally included in the calculations of the zinc-loaded form by adding a new residue in the amino acid sequence. This residue is formed from a chain of dummy atoms that have the van der Waals radii set to zero so they can freely penetrate into the protein and one atom with a radius of 1.4 Å, which mimics the zinc ion. The sulfur atoms of Cys ligands and $N^{\epsilon 2}$ of His-119 were linked to the metal ion through upper distance limits of 2.3 and 2.1 Å, respectively, on the basis of EXAFS data. This approach does not impose any fixed orientation of the ligands with respect to the zinc ion.

The 30 conformers with the lowest residual target function values were subjected to restrained energy minimization with AMBER 8.0 (22). NOE and torsion angle constraints were applied with force constants of 50 kcal mol^{-1} $Å^{-2}$ and 32 kcal mol^{-1} rad^{-2}, respectively. The force field parameters for the zinc(II) ion and the ligands were adapted from those already reported for similar zinc sites in zinc proteins and complexes (23–25). The quality of the structures was evaluated using the program PROCHECK and PROCHECK-NMR (26, 27). Structure visualization was done with the program MOLMOL (28).

RESULTS

Yeast Cox4 Is a Zinc-binding Protein—Four cysteine residues in the C-terminal domain of bovine CoxVb coordinate a single Zn(II) ion. Yeast Cox4 contains only three of the coordinating cysteine residues. No candidate ligand exists in the position of the fourth Cys from the bovine CoxVb sequence (8). To determine whether yeast Cox4 is a zinc-binding protein, an N-terminal truncate of yeast Cox4 was expressed in *E. coli*. The truncation removed 26 residues that contribute to the mitochondrial target sequence (29) and an additional 52 residues on the N-terminal side that in bovine CoxVb has an extended helical conformation (Fig. 1). The purified recombinant Cox4 (80 residues) was found to be a monomeric protein containing Zn(II) in a 1:1 ratio.

Zn(II) Coordination Sphere—Because Zn(II) is a d^{10} metal with no outer shell unpaired electrons, Zn(II) is spectroscopically silent. To address the coordination environment of yeast Cox4, Cd(II) was exchanged into Cox4 using ^{113}Cd. The ½ nuclear spin of ^{113}Cd allows facile detection by NMR. The cadmium nucleus has its magnetic field influenced by nearby and ligating atoms. NMR spectroscopy of the ^{113}Cd-Cox4 complex revealed a resonance at 664 ppm based on a $Cd(ClO_4)_2$ reference standard (Fig. 2*A*). This chemical shift position is suggestive of coordination by three sulfurs and one nitrogen/oxygen atom based on reference ^{113}Cd-substituted proteins (9). Three sulfur atoms are presumably provided by the three conserved cysteines in Cox4. Yeast Cox4 contains four histidines with one (His-119) positioned eight residues after the first cysteine with the remaining three in the C-terminal segment.

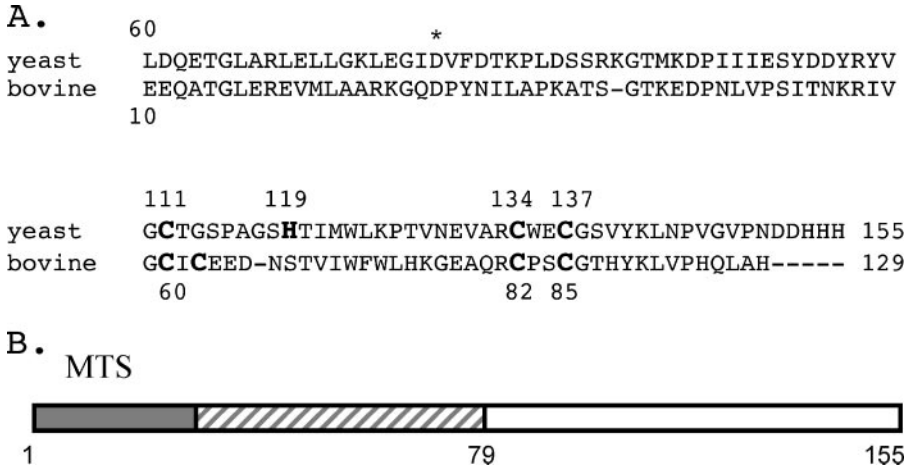

FIGURE 1. *Panel A*, comparison of yeast Cox4 and bovine CoxVb sequences. The *numbers* indicate the positions of the Zn(II) ligands. The *asterisk above* the yeast Cox4 sequence indicates the start of the sequence used in the structural determination. The construct used presently has a three residue N-terminal extension (MMA). *Panel B*, schematic of the portion of yeast Cox4 used in the structural studies (*open*, *unfilled box*). *MTS* refers to the mitochondrial target sequence.

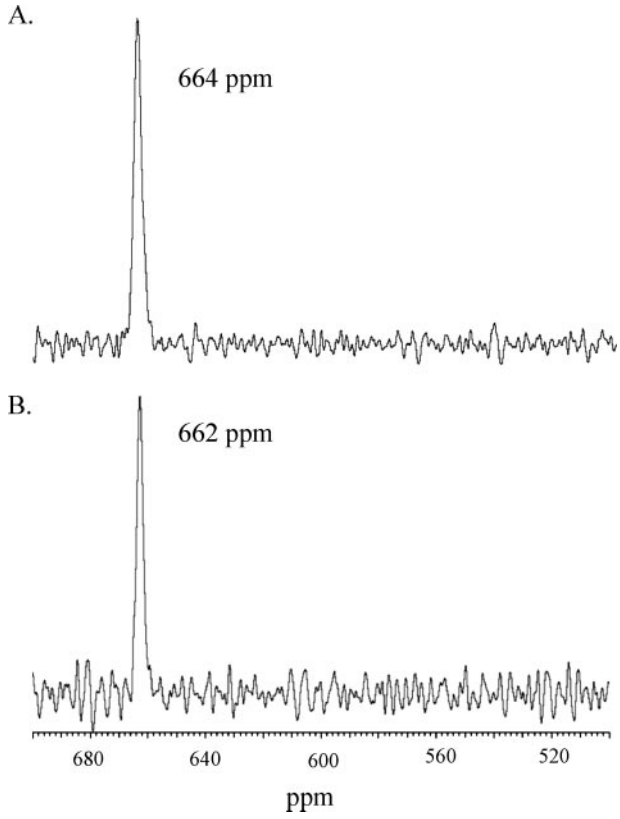

FIGURE 2. **^{113}Cd NMR of Cd-Cox4 and the Cd-Cox4 C-terminal truncate.** *Panel A*, the one-dimensional ^{113}Cd NMR spectrum of Cox4 protein at pH ≈ 7.3 in a 300 mM Tris 300 mM NaCl buffer. Cox4 was at ~1 mM with 1 mol eq of ^{113}Cd(II) incorporated in the previously denatured protein. *Panel B*, the one-dimensional ^{113}Cd NMR spectrum of the C-terminal Cox4 truncate (~1 mM) observed at a pH ≈ 7.3 in 200 mM Tris, 200 mM NaCl buffer. Both spectra were recorded on a Varian 500 MHz instrument.

A Cox4 construct was prepared that lacked the last 6 C-terminal residues (NDDHHH), removing all histidyl residues except His-119. Purification of the recombinant C-terminal truncate revealed 1 mol eq of bound Zn(II). Exchanging the Zn((II) with ^{113}Cd(II) resulted in a complex with bound Cd(II). NMR of the ^{113}Cd-Cox4 truncate showed a resonance of 662 ppm (Fig. 2*B*). The similar chemical shift of the Cd-Cox4 C-terminal truncate suggests that the C-terminal His residues do not contribute to Zn(II) coordination, leaving His-119 as the likely nitrogen donor to Zn(II) in the WT protein.

The C-terminal His-rich sequence in Cox4 is able to bind an additional Zn(II). Cox4 purified from *E. coli* cultured in the presence of supplemental $ZnCl_2$ was recovered with 1.7 mol eq of bound Zn(II), whereas a Cox4 truncate lacking the C-terminal 6 residues bound only a single Zn(II) ion. Zn(II) binding to the C-terminal His-rich motif results in Cox4 aggregation. Titration of ^{15}N-labeled Cox4 with additional $ZnSO_4$ results in a broadening of the resonances, whereas a similar titration with the C-terminal truncate failed to show any resonance broadening (supplemental Fig. S1).

EXAFS analysis of the C-terminal truncate Zn-Cox4 complex was used to confirm the coordination environment of the metal (Fig. 3). Quantitative analysis of the EXAFS using curve fitting indicated a mixed coordination environment with three sulfurs at 2.32 Å and either 1 or 2 nitrogen or oxygen ligands at 2.02 Å. The four-coordinate and five-coordinate alternatives gave equivalent fits, but which of these is present can be revealed by comparison of bond lengths. Examination of the Cambridge Crystal Structure data base indicates that the bond lengths are fully consistent with a four-coordinate species, whereas a five-coordinate alternative is precluded as this would give much longer bond lengths for both Zn–S and Zn–O/N ligands. Fourier transform peaks near 3 and 4 Å are often taken as a fingerprint of histidine coordination. These are not clearly observed in our data; however, their absence does not definitely preclude His coordination, especially in the presence of very large backscattering from three sulfur ligands.

Mutagenesis Analysis of Zinc Ligands in Cox4—To assess the role of His-119 and the three conserved Cys residues in Zn(II) coordination and function, mutagenesis analysis was undertaken. Yeast (*cox4*Δ) transformed with a vector containing either WT *COX4* or a mutant gene was tested on glycerol-containing medium for respiratory growth. Cox4 mutants with Cys > Ser substitutions at the three conserved positions individually failed to support cell growth on glycerol-containing medium regardless of whether the mutant gene was expressed on a low copy (Fig. 4*A*) or high copy (data not shown) vector, whereas the WT *COX4* rescued glycerol growth. The addition of 8 mM $ZnCl_2$ to the mutant cultures failed to support glycerol growth (data not shown). The Cys > Ser mutant variants of Cox4 are each unstable proteins and fail to accumulate (Fig. 4*B*).

CcO fails to assemble in cells lacking Cox4 (12). To test whether assembly is precluded in cells with Cys > Ser mutant

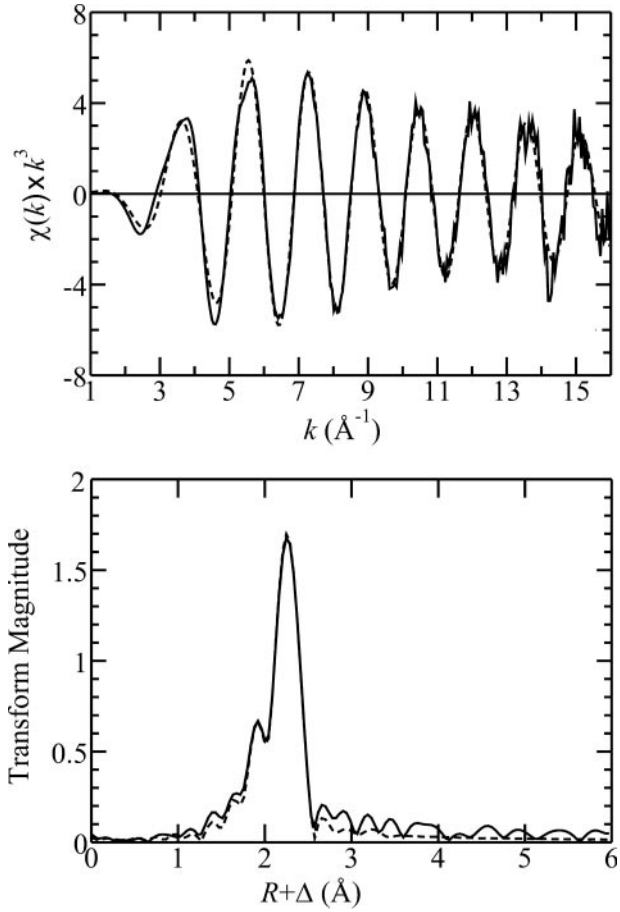

FIGURE 3. **EXAFS spectra (*solid line*) plus best fit (*broken line*) (*upper panel*) and corresponding EXAFS Fourier transforms (Zn–S phase-corrected) (*lower panel*).** The two clearly observed Fourier transform peaks at ~2 and 2.3 Å correspond to the Zn–O/N and Zn–S interactions, respectively.

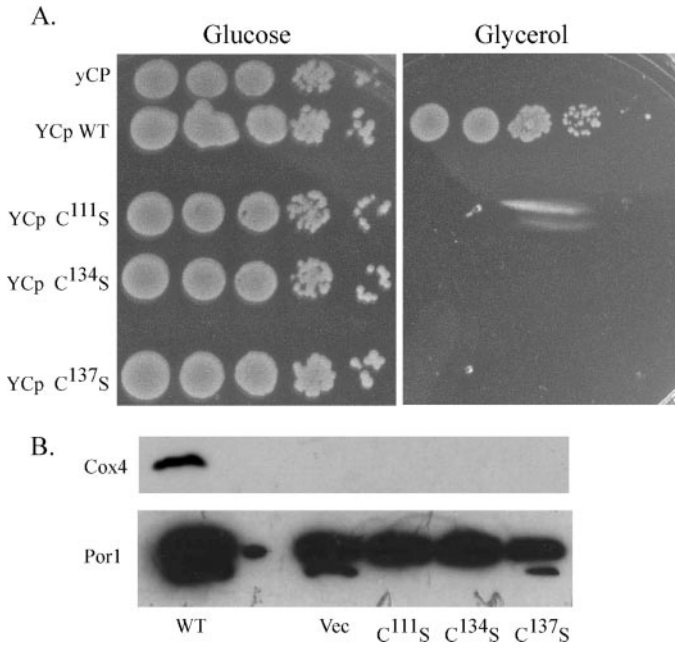

FIGURE 4. ***In vivo* complementation test of Δ*cox4* cells by Cox4 Cys mutants.** *Panel A*, low copy YCp plasmids encoding WT Cox4 or mutant proteins with individual Cys to Ser mutants for Cys-111, Cys-134, and Cys-137 were transformed into a Δ*cox4* yeast cells. Transformants were cultured as serial dilutions on glucose and glycerol medium. *Panel B*, immunodetection of Cox4 and variants from isolated mitochondria. The mitochondrial fractions were trichloroacetic acid-precipitated to provide equal total protein loads for each lane. The samples were analyzed on 12.5% SDS-PAGE with subsequent transfer to nitrocellulose for Cox4 and porin detection.

Cox4, mitochondria purified from *cox4*Δ cells containing C111S Cox4 were subjected to SDS-PAGE and probed for Cox2. No Cox2 was detected in the mutant cells, although a robust Cox2 band was detected in WT cells (data not shown).

Mutational analysis was carried out on His-119 to evaluate its importance in Cox4 function. Alanine, aspartate, and cysteine substitutions were engineered. Aspartate and cysteine substitutions were attempted to provide a potential Zn(II) donor ligand. Each His mutant Cox4 enabled cells to propagate on glycerol medium when overexpressed but not when expressed from a low copy plasmid (Fig. 5*A*), and as expected, mutant protein levels were detected (Fig. 5*B*). Partial CcO activity was observed in cells containing the high copy mutants (Fig. 5*C*). In contrast, cells harboring either the H119D or H119C mutant Cox4 exhibited limited growth on zinc-supplemented glycerol medium when the mutants were on low copy plasmids (Fig. 5*A*). These results are consistent with low affinity Zn(II) binding to the H119D and H119C mutant Cox4 proteins. Consistent with the ^{113}Cd NMR studies above, the C-terminal truncate lacking the C-terminal 3 His residues resembled WT Cox4 in respiratory growth (data not shown). These results implicate His-119 as the fourth Zn(II) ligand in yeast Cox4.

Biophysical Studies on the H119D Mutant Cox4—Because the H119D mutant Cox4 was less stable for metal substitution, we elected to use Co(II) electronic spectroscopy as a more rapid analysis probe to monitor the coordination environment. Wild-type and mutant Cox4 were converted to Co(II) complexes for UV-visible spectroscopy. The absorption in the visible range between 550 and 700 nm arises from *d-d* transitions of unpaired electrons and provides information on the Co(II) coordination environment (10). The absorption envelope of Co-Cox4 lies between 600 and 720 nm and is typical of a distorted tetrahedral environment with coordination by three sulfurs and one nitrogen ligand based on known Co^{+2}-substituted proteins (Fig. 6). The molar absorptivity greater than 500 M^{-1} cm^{-1} is consistent with three sulfurs. The absorption envelope for the *d-d* transitions of Co-Cox4 H119D is red-shifted compared with the envelope of the wild-type protein (Fig. 6). The wild-type construct has maxima at 648 and 698 nm and a prominent shoulder at 620 nm, whereas the H119D mutant displays absorbance maxima near 700 and 720 nm. If His-44 were the fourth ligand in Cox4, the H119D substitution would now present an oxygen donor that is a weaker field ligand compared with a nitrogen atom. The lower crystal field splitting energy would make the *d-d* transition less energetic, resulting in a red shift of the spectral envelope. Cobalt electronic spectroscopy data substantiates His-119 as the fourth ligand.

Solution Structure of Zn-Cox4—The 80-residue Zn-Cox4 complex was subjected to multidimensional NMR spectroscopy for structure determination. His-119 was confirmed to be the fourth Zn(II) ligand by virtue of the chemical shift difference of ^{15}N resonances of the imidazole ring of a histidine residue for coordinated *versus* noncoordinated His residues

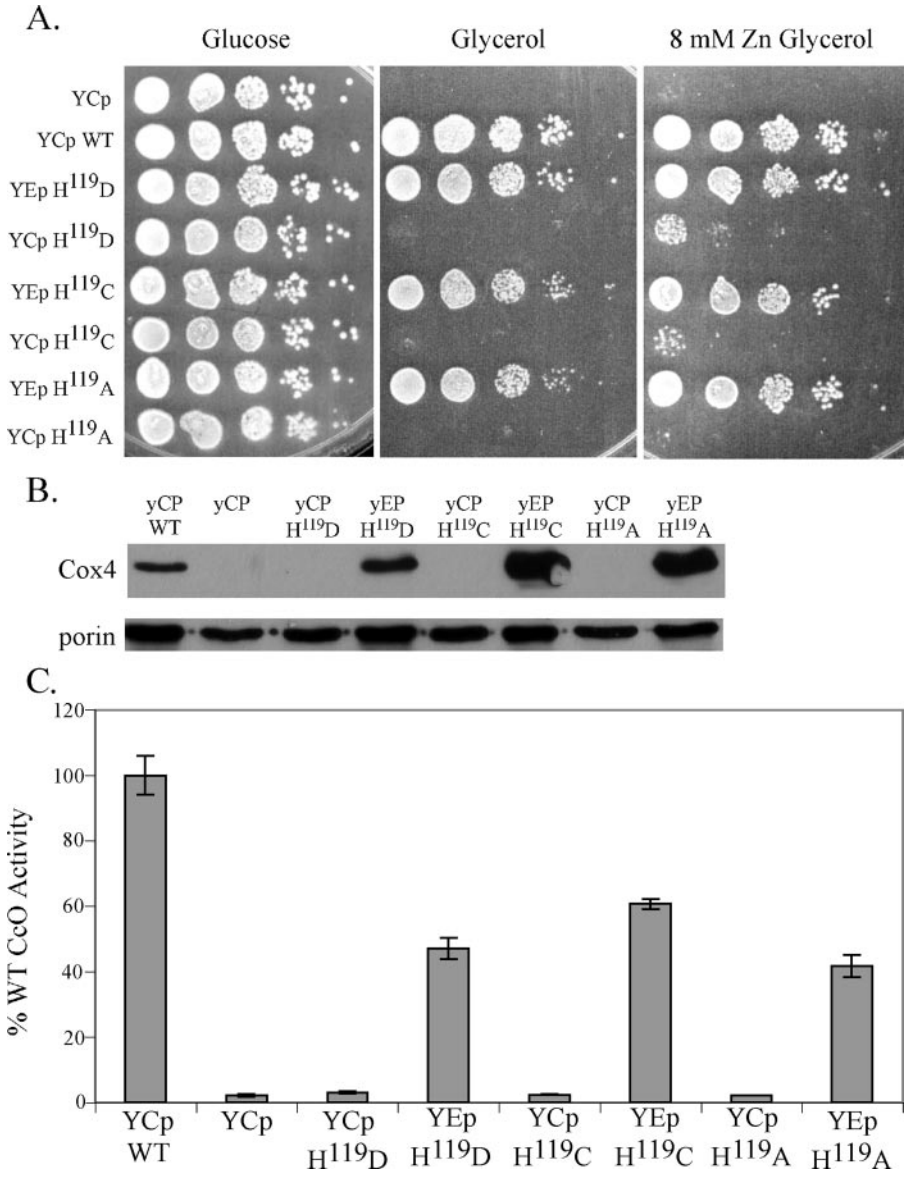

FIGURE 5. ***In vivo* complementation test of Δ*cox4* cells by Cox4 His-119 mutants.** *Panel A*, low copy (YCp) and high copy (YEp) plasmids encoding WT Cox4 or His-119 mutant variants were transformed into a Δ*cox4* yeast. Growth of transformants is shown as serial dilutions on glucose, glycerol plates, and glycerol plates supplemented with 8 mM $ZnCl_2$. *Panel B*, immunodetection of Cox4 and mutant variants from isolated mitochondria. The mitochondrial fractions were trichloroacetic acid-precipitated to provide equal total protein loads for each lane. The samples were analyzed on 12.5% SDS-PAGE with subsequent transfer to nitrocellulose for Cox4 and porin detection. *Panel C*, CcO activity of cells containing WT Cox4 or His mutant variants is expressed as a percentage of the WT Cox4 activity. The *error bars* are the error between a set of three separate measurements for each sample prepared.

(about 220 ppm for the metal-bound nitrogen *versus* 180 or 250 ppm, the two latter values depending on whether the nitrogen is protonated or not) (31). The chemical shifts for $N^{\delta 1}$ and $N^{\epsilon 2}$ of His-119 are 173.2 and 216.2 ppm, respectively (Fig. 7), consistent with the presence of a coordination bond between $N^{\epsilon 2}$ of His-119 and the Zn(II) ion. $^{1}H,^{15}N$ HSQC experiments optimized for the detection of the $^{2}J_{NH}$ couplings in the imidazole ring performed on Zn-Cox4 at room temperature also show that His-119 is protonated on $N^{\delta 1}$.

The $^{1}H,^{15}N$ HSQC spectrum of Zn-Cox4 recorded at 298 K is indicative of an essentially folded protein with well dispersed amide signals (Fig. 7). The solution structure of Zn-Cox4, as obtained by using 1172 meaningful upper distance limits and 46 angle restraints, has after energy minimization a root mean square deviation to the mean structure (residues 10–70) of 0.78 Å (with a variability of 0.20 Å) for the backbone and 1.18 Å (with a variability of 0.17 Å) for the heavy atoms. The conformational and energetic analysis of Zn-Cox4 structure is reported in supplemental Table S3.

The Zn-Cox4 fold contains five β strands organized in one sheet of 2 and another of 3 strands involving residues 98–100 (β1), 109–111 (β2), 122–124 (β3), 131–133 (β4), and 140–143 (β5) (Fig. 8). Metal ligands are located in two opposite regions at one edge of the β-sheets with their side chains pointing in the interior of the protein core where the metal is located (Fig. 8). The zinc ion is, therefore, buried within the protein core with no solvent accessibility, suggesting that zinc plays essentially a structural role stabilizing the Cox4 fold. Zn-Cox4 has the same fold as that of the mammalian homolog Zn-CoxVb, with all β-strands essentially superimposed (Fig. 8, *bottom*). The length of β-strands of Zn-Cox4 is, however, reduced with the respect to that of Zn-CoxVb. The presence of a Pro residue (Pro-126) in Cox4 sequence contributes to the shortening of strands β2 and β3, as its insertion breaks the network of hydrogen bonds necessary for the β-sheet formation. Pro-126 is not conserved in CoxVb but is replaced by Leu-74 that is part of the hydrophobic interaction in the protein core of Zn-CoxVb, thus likely favoring a longer β3 strand. The zinc ion and the three conserved Cys ligands of the two orthologs are similarly arranged in the two structures (Fig. 8). The fourth ligand, Cys-137 in Zn-CoxVb and His-119 in Zn-Cox4, is located in loop 2 in both structures but in a different position. This loop in the two structures assumes a different structural arrangement. The loop in Zn-Cox4 approaches the zinc site in the region containing His-119, whereas the corresponding region in Zn-CoxVb is exposed toward the solvent. Conversely, the loop region containing C62 in Zn-CoxVb is spatially close to the Zn(II) site, but it is distal from in Zn-Cox4 (Fig. 8). Therefore, loop 2 adapts its conformation accordingly to the different sequence position of the metal ligand. Consistent with this analysis, limited amino acid conservation is observed in the yeast and bovine primary sequences of this loop region.

The core of the Zn-Cox4 is characterized by a few hydrophobic interactions involving 6 residues Ile-100, Val-109, Met-122, Leu-124, Tyr-141, and Leu-143, which are conserved in the Zn-CoxVb structure (residues Val-49, Val-58, Ile-70, Phe-72, Tyr-89, Leu-91) (Fig. 9). In addition, hydrophobic residues (Tyr-108, Ile-121, Trp-123 in Zn-Cox4 and Ile-57, Val-69, Trp-71 in Zn-CoxVb) are conserved on the solvent-exposed face of the two-stranded β-sheet. These residues form hydrophobic interactions with Leu-492, Leu-495, and Phe-505 residues located at the C terminus of the Cox1 subunit in the bovine CcO structure (Fig. 9), suggesting that these conserved hydrophobic residues play an important role in the Cox4-Cox1 interaction also in yeast. This region in both Zn-Cox4 and Zn-CoxVb is indeed essentially apolar, at variance with the corresponding residues in the three-stranded β-sheet.

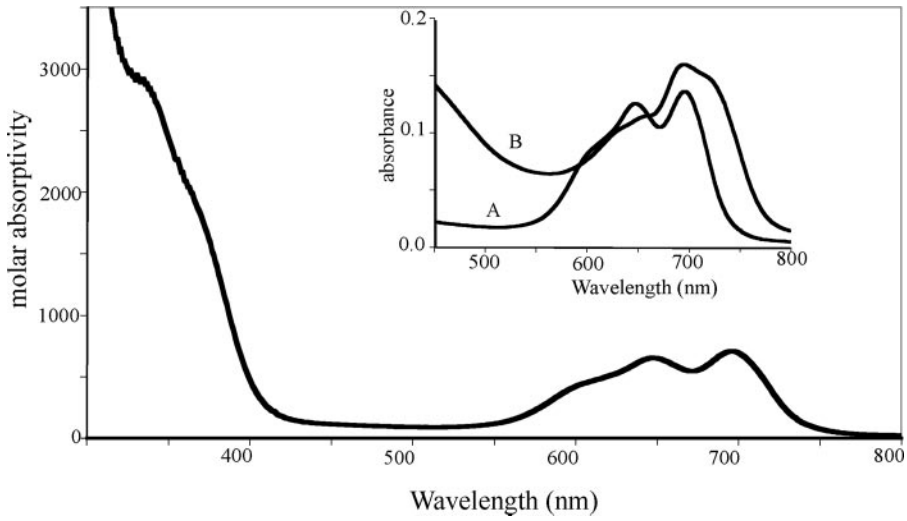

FIGURE 6. **Cobalt electronic spectroscopy of the C-terminal Cox4 truncate and the H119D mutant variant.** The UV-visible spectra of a 0.2 mM Cox4 solution reconstituted with 1 mol eq of Co(II) under anaerobic conditions. The molar absorptivity in the visible region of for the *d-d* transitions are between 505 and 708 mM^{-1} cm^{-1}. *Inset*, the overlay of the visible spectra of 0.2 mM Cox4 (*sample A*) and 0.5 mM H119D mutant Cox4 (*sample B*). Both samples were prepared anaerobically. The H119D mutant Cox4 was unstable and precipitated with time leading to the elevated base line.

DISCUSSION

The Zn(II)-binding Cox4 is one of the two globular subunits of CcO facing the matrix side of the IM, the other being Cox6. Cox4 is the only

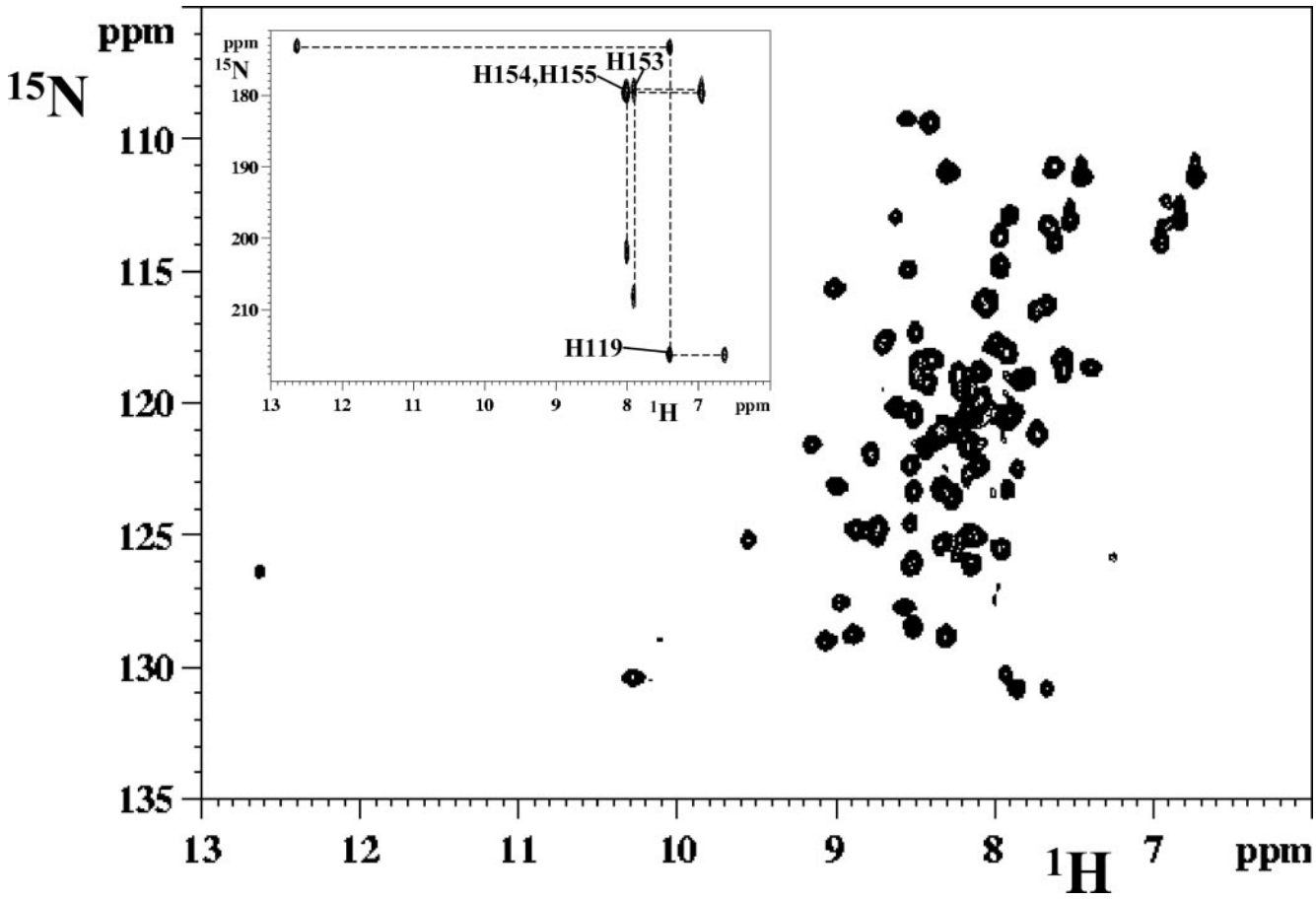

FIGURE 7. **$^1H,^{15}N$ HSQC spectrum recorded on Zn-Cox4 at protein concentration of 1.0 mM in 50 mM phosphate 200 mM NaCl buffer.** The spectra were collected at 298 K and pH 6.9 on a spectrometer equipped with cryo-probe and operating at 500 MHz. In the *inset* $^1H,^{15}N$ HSQC spectrum optimized for the detection of $^2J_{NH}$ of histidine rings is shown. In this experiment the INEPT delay was set to 22 ms.

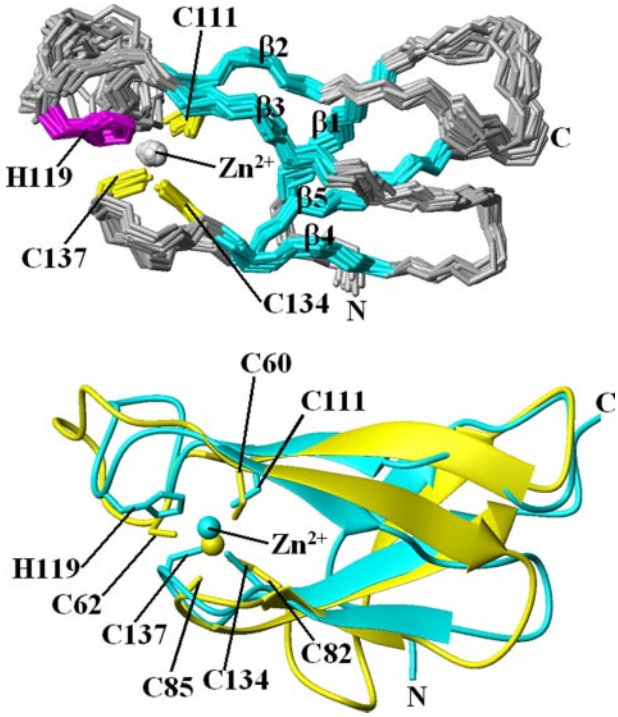

FIGURE 8. *Top*, representation of the bundle of the 20 lowest energy conformers of Zn-Cox4. The β-strands elements are shown in *cyan*. The side chains of His-119, Cys-111, Cys-134, Cys-137, and the Zn^{2+} ion are also shown. *Bottom*, structure of the Zn-Cox4 (*cyan*) compared with that of bovine Zn-CoxVb (*yellow*). The zinc ligands of both proteins are also reported in *cyan* and *yellow*, respectively.

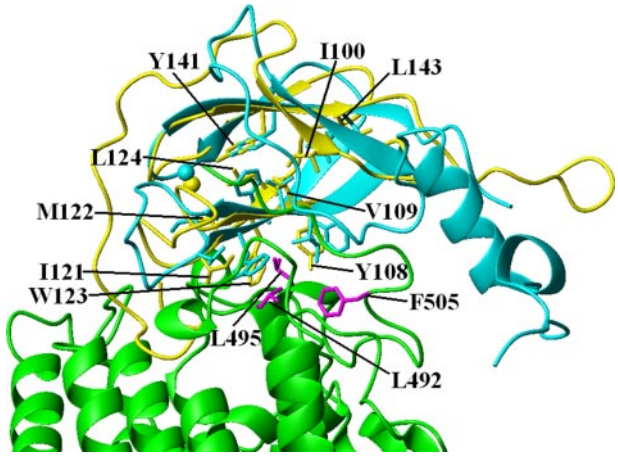

FIGURE 9. **Structure of Zn-Cox4 (*yellow*) superimposed, fitting over secondary structure elements with the Zn-CoxVb subunit (*cyan*) in the bovine CcO structure.** Cox1 subunit is shown in *green*. Hydrophobic residues conserved in both Cox4 and CoxVb are shown in *yellow* and *cyan*, respectively. Leu-492, Leu-495, and Phe-505 residues of Cox1 involved in hydrophobic interactions with CoxVb subunit are also shown in *violet*.

cofactor-containing subunit that is not directly part of the catalytic core. The role of Zn(II) binding in Cox4 has not been previously investigated. We show presently that CcO assembly and stabilization is dependent on the presence of Cox4 and on Zn(II) coordination in Cox4. Mutant proteins with any of the three Zn-coordinating Cys residues mutated are nonfunctional and fail to lead to an assembled CcO complex as is the case in cells depleted of Cox4 (7, 12). Furthermore, the structure of Cox4 is dependent on bound Zn(II). The HSQC spectrum of apoCox4 is collapsed (data not shown). Thus, Zn(II) binding to Cox4 is essential to the stability of Cox4 and subsequently CcO.

Yeast Cox4 differs from the bovine ortholog in lacking one of the Zn(II)-binding Cys residues (8). No candidate ligand exists in the position of the fourth conserved Cys from the bovine ortholog. ^{113}Cd NMR spectroscopy of Cox4 suggested that a single His residue contributed to the Zn(II) coordination sphere. Because the chemical shift of the ^{113}Cd-Cox4 protein did not change upon deletion of the C-terminal 6 residues containing 3 of the 4 His residues present in the protein, His-119 was implicated as the Zn(II) ligand. This prediction was confirmed by the chemical shift of the His-119 imidazole ring nitrogen and the solution structure determination. The N^{ϵ} rather than the N^{δ} ring nitrogen is coordinated to Zn(II). The N^{ϵ} is the usual donor atom in proteins with structural Zn(II) sites. The N^{δ} nitrogen is protonated in Cox4, and it is commonly hydrogen-bonded to water or a protein carboxylate. In Cox4, the N^{δ} is not hydrogen-bonded to a protein residue, leaving open the possibility that it is hydrogen-bonded to solvent or to a Cox1 residue.

Whereas Cys > Ser mutants in Cox4 are nonfunctional, H119A, H119C, and H119D Cox4 variants were functional when overexpressed. The partial function of CcO containing a H119D Cox4 suggests that Zn(II) coordination may persist in this mutant. The H119D Cox4 mutant is isolated recombinantly with a lower Zn(II) stoichiometry, and the residual Zn(II) is labile to dialysis. Supplemental $ZnCl_2$ enhanced growth of *cox4*Δ cells harboring the H119D but not the H119A mutant Cox4, consistent with the aspartate serving as a weak ligand. The Cys > Ser mutants of Cox4 could not be purified as the recombinant mutant proteins were highly aggregated.

It is not clear whether Cox4 has a functional role in addition to stabilizing CcO. Its presence on the matrix side of the IM suggests a few possibilities. CcO is subject to feedback regulation by ATP (32, 33), and ATP inhibition is expected to occur on the matrix side of CcO, leaving subunits Cox4 and Cox6 as candidate inhibitory sites. Allosteric ATP inhibition of CcO is only observed in the eukaryotic enzyme, suggesting that the peripheral subunits may mediate this regulation. Multiple ATP binding sites were predicted, although the only subunit clearly implicated is mammalian CoxIV (yeast Cox5a), which has a small matrix domain in addition to an IM spanning sequence. This subunit was implicated as one ATP interaction site of CcO on the basis of photoaffinity labeling studies (34). To determine whether yeast Cox4 is also an ATP binding subunit, an $^{1}H,^{15}N$ HSQC NMR study was carried out in the presence and absence of varying concentrations of ATP. No perturbation in Cox4 resonances was observed.

As mentioned, the C-terminal His-rich motif of Cox4 is capable of binding an additional Zn(II) ion, and the resulting complex is susceptible to aggregation (supplemental Fig. S1). The C-terminal tail of bovine CoxVb is in close juxtaposition to the His-rich N-terminal sequence of Cox3 that is suggested to be important in proton pumping through the D-pathway (3). Because Zn(II) binding is known to inhibit the D-pathway of proton pumping (35), the possibility exists that the C-terminal His-rich segment of Cox4 may also be involved in proton collection for proton pumping. In support of this postulate, Cox4

residues His-153 and His-155 show significant perturbations in chemical shift as a function of pH (supplemental Fig. S2).

Respiratory regulation from a high membrane potential in addition to allosteric ATP regulation is postulated. Conditions of high membrane potential (>150 mV) are predicted to increase ROS production (36). One attractive mechanism to dissipate a high membrane potential yielding high ROS levels is a putative ROS-mediated inhibition of CcO. The zinc-containing Cox4 may be a candidate ROS sensor through a zinc-redox switch mechanism analogous to the Hsp33 chaperone in *E. coli* (37, 38). Hsp33 is a chaperone protein that is maintained in its inactive state as a zinc-binding protein. Under oxidizing conditions Hsp33 is activated to gain molecular chaperone activity. The activation process involves a major conformational change accompanying Zn(II) displacement and disulfide formation. Redox activity of sulfur ligands in Zn(II) sites, designated as a zinc redox switch, is postulated to be a significant redox regulation mechanism. Although the zinc site in Cox4 is buried with no solvent accessibility, the sulfur moiety of bovine CoxVb Cys-62 is partially solvent-accessible, leaving open the possibility that Cox4 may represent a zinc-redox sensor for mitochondrial ROS. The other two cysteinyl sulfurs are largely buried and unlikely to be accessible to ROS. Reversible oxidation of the yeast Cox4 Cys-137 may modulate CcO activity and control the mitochondrial membrane potential. Future experiments will address this candidate functional role.

Acknowledgments—Portions of this work were carried out at the Stanford Synchrotron Radiation Laboratory, which is funded by the U.S. Department of Energy, Office of Basic Energy Sciences and Office of Biological and Environmental Sciences, and the National Institutes of Health, National Center for Research Resources. We acknowledge the assistance of Jay Olson, Dr. Jack Skalicky, Dr. Peter Flynn, and Greg Keller.

REFERENCES

1. Yoshikawa, S. (2002) *Adv. Protein Chem.* **60,** 341–395
2. Tsukihara, T., Aoyama, H., Yamashita, E., Tomizaki, T., Yamaguchi, H., Shinzawa-Itoh, K., Hakashima, R., Yaono, R., and Yoshikawa, S. (1995) *Science* **269,** 1069–1074
3. Hosler, J., Ferguson-Miller, S., and Mills, D. A. (2006) *Annu. Rev. Biochem.* **75,** 165–187
4. Yoshikawa, S., Shinzawa-Itoh, K., and Tsukihara, T. (2000) *J. Inorg. Biochem.* **82,** 1–7
5. Gilderson, G., Salomonsson, L., Aagaard, A., Gray, J., Brezezinski, P., and Hosler, J. (2003) *Biochemistry* **42,** 7400–7409
6. Poyton, R. O., and McEwen, J. E. (1996) *Annu. Rev. Biochem.* **65,** 563–607
7. McEwen, J. E., Ko, C., Kloeckner-Gruiissem, B., and Poyton, R. O. (1986) *J. Biol. Chem.* **261,** 11872–11879
8. Capaldi, R. A. (1990) *Annu. Rev. Biochem.* **59,** 569–596
9. Coleman, J. E. (1993) *Methods Enzymol.* **227,** 16–43
10. Bertini, I., and Luchinat, C. (1984) in *Advances in Inorganic Biochemistry* (Eichhorn, G. L., and Marzilli, L. G., eds) Elsevier Science Publishing Co., Inc., New York
11. Maret, W., and Vallee, B. L. (1993) *Methods Enzymol.* **226,** 52–71
12. Glerum, D. M., and Tzagoloff, A. (1997) *FEBS Lett.* **412,** 410–414
13. Diekert, K., De Kroon, A. I. P. M., Kisplal, G., and Lill, R. (2001) *Methods Cell Biol.* **65,** 37–51
14. Bradford, N. M. (1976) *Anal. Biochem.* **72,** 248–254
15. Cramer, S. P., Tench, O., Yocum, M., and George, G. N. (1988) *Nucl. Instrum. Methods Phys. Res. A* **266,** 586–591
16. Rehr, J. J., Albers, R. C., and Zabinsky, S. I. (1992) *Phys. Rev. Lett.* **69,** 3397–3400
17. Keller, R. (2004) *The Computer Aided Resonance Assignment Tutorial*, 1st Ed., Verlag, Cantina, Switzerland
18. Herrmann, T., Guntert, P., and Wuthrich, K. (2002) *J. Biomol. NMR* **24,** 171–189
19. Herrmann, T., Guntert, P., and Wuthrich, K. (2002) *J. Mol. Biol.* **319,** 209–227
20. Guntert, P. (2004) *Methods Mol. Biol.* **278,** 353–378
21. Wishart, D. S., and Sykes, B. D. (1994) *J. Biomol. NMR* **4,** 171–180
22. Case, D. A., Cheatham, T. E., Darden, T., Gohlke, H., Luo, R., Merz, K. M. J., and Onufriev, C. (2005) *J. Comput. Chem.* **26,** 1668–1688
23. Banci, L., Bertini, I., Ciofi-Baffoni, S., Finney, L. A., Outten, C. E., and O'Halloran, T. V. (2002) *J. Mol. Biol.* **323,** 883–897
24. Suarez, D., and Merz, K. M. J. (2001) *J. Am. Chem. Soc.* **123,** 3759–3770
25. Banci, L. (2003) *Curr. Opin. Chem. Biol.* **7,** 143–149
26. Laskowski, R. A., Rullmannn, J. A., MacArthur, M. W., Kaptein, R., and Thornton, J. M. (1996) *J. Biomol. NMR* **8,** 477–486
27. Laskowski, R. A., MacArthur, M. W., Moss, D. S., and Thornton, J. M. (1993) *J. Appl. Crystallogr.* **28,** 283–291
28. Koradi, R., BIlleter, M., and Wuthrich, K. (1996) *J. Mol. Graph.* **14,** 51–55
29. Taanman, J. W., and Capaldi, R. A. (1992) *J. Biol. Chem.* **267,** 22481–22485
30. Deleted in proof
31. Chen, Y. L., Park, S., Thornburg, R. W., Tabatabai, L. B., and Kintanar, A. (1995) *Biochemistry* **34,** 12265–12275
32. Beauvoit, B., Bunoust, O., Guerin, B., and Rigoulet, M. (1999) *Eur. J. Biochem.* **263,** 118–127
33. Lee, I., Bender, E., Arnold, S., and Kadenbach, B. (2001) *Biol. Chem.* **382,** 1629–1636
34. Bisson, R., Schiavo, G., and Montecucco, C. (1987) *J. Biol. Chem.* **262,** 5992–5998
35. Aagaard, A., Namslauer, A., and Brzezinski, P. (2002) *Biochim. Biophys. Acta* **1555,** 133–139
36. Ludwig, B., Bender, E., Arnold, S., Huttemann, M., Lee, I., and Kadenbach, B. (2001) *Chembiochem* **2,** 392–403
37. Jacob, U., Eser, M., and Bardwell, J. C. (2000) *J. Biol. Chem.* **275,** 38302–38310
38. Ilbert, M., Graf, P. C., and Jakob, U. (2006) *Antioxid. Redox Signal.* **8,** 835–846

The Characterization and Role of Zinc Binding in Yeast Cox4

H. Jerome Coyne III, Simone Ciofi-Baffoni, Lucia Banci, Ivano Bertini, Limei Zhang, Graham N. George and Dennis R. Winge

J. Biol. Chem. 2007, 282:8926-8934.
doi: 10.1074/jbc.M610303200 originally published online January 10, 2007
